Research Article Vol. 16, No. 5 / 1 May 2025 / Biomedical Optics Express 2198
Biomedical Optics EXPRESS

Gold nanoparticle decorated flexible carbon cloth for sensitive detection of 2, 6-pyridine dicarboxylic acid by surface-enhanced Raman scattering

LIN CHEN,[1,†] DONG YANG,[2,†] XIANGLONG BIAN,[1] QIANFENG XIA,[1] PAUL K CHU,[3] AND TINGWEI HU[1,4,*]

[1]NHC Key Laboratory of Tropical Disease Control, School of Tropical Medicine, Hainan Medical University, Haikou 571199, Hainan, China
[2]School of Biomedical Information and Engineering, Hainan Medical University, Haikou 571199, Hainan, China
[3]Department of Physics, Department of Materials Science and Engineering, and Department of Biomedical Engineering, City University of Hong Kong, Tat Chee Avenue, Kowloon, Hong Kong SAR, China
[4]State Key Laboratory for Mechanical Behavior of Materials, Xi'an Jiaotong University, Xi'an 710049, Shaanxi, China
[†]Lin Chen and Dong Yang contributed equally to this work.
[*]htingwei1236@mail.xjtu.edu.cn

Abstract: The lethal bacterium of bacillus anthracis has been recognized as a kind of formidable biological warfare agent, and the biomarker of 2, 6-pyridine dicarboxylic acid (DPA) is a crucial component of the protective layer of anthrax spore. The development of an efficient and sensitive detection method for DPA is necessary to prevent the potential biological threats. In this experiment, the porous carbon cloth (CC) and different sizes of gold nanoparticles (AuNPs) are composited together to construct a flexible SERS substrate of AuNPs@Au/CC. The high surface-enhanced Raman scattering (SERS) performance of AuNPs@Au/CC substrate is assessed by the probe molecule of Rhodamine 6 G (R6 G). During the detection of DPA, the SERS substrate of AuNPs@Au/CC exhibits a linear detection range from 10^{-7} M to 10^{-13} M with a limit of detection (LOD) of 1.58×10^{-13} M. The flexible CC substrate decorated with different sizes of AuNPs can facilitate the contact of DPA molecules and enhance the Raman signal. It provides potential application for the rapid and sensitive DPA detection for preventing the biological threats.

1. Introduction

Anthrax is a serious and acute infectious disease usually caused by inhalation of pathogenic spores of Bacillus anthracis. This anthrax spore is a Gram-positive bacterium that can survive in harsh environments for many years and has a strong environmental resilience. Bacillus anthracis can invade human body through skin wounds, respiratory tract or digestive tract, causing different types of anthrax disease [1,2]. When these spores are atomized, they can become airborne and become a potential biological weapon, posing a serious threat to public health [3]. If more than 10^4 spores are inhaled and are not treated effectively within 24 to 28 hours, the mortality rate is extremely high [4]. For example, the bacteria has caused multiple deaths during the anthrax attacks in the United States in 2001, highlighting its biological threat to national security as a means of bioterrorism [5]. Because of its high pathogenicity, lethality and infectivity, Bacillus anthracis has been considered as a kind of potentially deadly biological warfare agent and attracted globally attention [6–8].

#562344 https://doi.org/10.1364/BOE.562344
Journal © 2025 Received 21 Mar 2025; revised 16 Apr 2025; accepted 16 Apr 2025; published 1 May 2025

Biomedical Optics EXPRESS

Traditional methods of diagnosing Bacillus anthracis rely on a process of microbial culture, which typically takes 12 to 48 hours and significantly limits the rapid detection of Bacillus anthracis. 2, 6-pyridine dicarboxylic acid (DPA) is the crucial component of the protective layer of anthrax spore, which not presents in other non-spore-producing bacteria and molds. The DPA content in spores accounts for 5% to 15% of the dry weight, which has been considered as the key biomarker of Bacillus anthracis [9,10]. DPA plays a vital role in the formation, stability, and tolerance of the spores of Bacillus anthracis. It endows the spores with extremely strong environmental tolerance, enabling them to withstand external physical and chemical factors and thus survive in adverse environments. The spores will wait for suitable conditions to germinate again and trigger infection. Therefore, DPA is not only an important component of the spores of Bacillus anthracis, but also one of the key factors of its uniqueness and pathogenicity. Considering the substantial threat that anthrax spores pose to both humans and animals globally, precise detection of DPA is paramount for ensuring biosecurity. Currently, varieties of analytical techniques has been documented for detecting DPA, including immunoassay [11,12], gas chromatography-mass spectrometry (GC-MS) [13,14], polymerase chain reaction (PCR) [15,16], colorimetric titration [17], fluorescence-based methods [18,19], and other approaches. The immunoassay exhibits moderate speed and reasonable sensitivity when detecting Bacillus anthracis, however, it has limitations as it cannot identify pathogens without antibodies and incurs significant costs [11]. GC-MS possesses exceptional sensitivity and selectivity when it comes to detecting and identifying bacteria. However, it entails significant sample pretreatment and necessitates a certain level of technical expertise and experience [13]. The PCR method possesses the capability to distinguish Bacillus anthracis from other bacillus species, albeit with a comparatively slow analysis speed [16]. The colorimetric sensors can indeed be employed for visual detection purposes, but, accurately quantifying the DPA concentration using these sensors remains challenging [17]. The fluorescence sensor has the capability of sensitivity and rapid detection for DPA, but, its preparation process is relatively intricate [20]. Despite demonstrating their efficacy in detecting DPA, these techniques still grapple with significant challenges, including analysis speed, cost and operational complexity [11,16,17]. Hence, it require urgent attention and immediate necessity for the creation of an ultra-sensitive, rapid, reusable, portable and economically viable biochemical sensor platform.

In recent years, the technology of surface-enhanced Raman scattering (SERS) has been utilized for the detection of the biomarker DPA associated with Bacillus anthracis. The sensitivity and specificity during DPA detection have been significantly improved. For example, Jiang et al. has developed an economical and readily available SERS substrate derived from natural organic matrix with impregnated silver nanoparticles (AgNPs) [21]. This SERS substrate enables precise quantitative detection of DPA within a linear range spanning from 40 nM to 1000 nM, achieving the limit of detection (LOD) of 8.62 nM [21]. Naqvi et al. has fabricated an ultra-sensitive and reusable SERS sensor through layered gold nanoparticles (AuNPs), which can achieve an impressive LOD of 0.83 pg/L for DPA detection [22]. Moreover, flexible SERS substrates are becoming increasingly favored due to the real-time detection capability for probe molecular without supplementary extraction procedures [23]. Carbon cloth (CC) boasts the advantages of exceptional conductivity, physical flexibility and durability, making it a highly affordable flexible SERS substrate. For example, Yao et al. has prepared a highly sensitive CC-based SERS substrate modified with gold nanoparticles, achieving a very low LOD for several kinds of molecular [24]. Therefore, SERS technology has been widely applied in the field of biomedical detection, offering significant advantages in enhancing sensitivity, specificity, and convenience [25,26].

The porous structure of flexible CC facilitates rapid analyte adsorption, thereby enhancing the speed and efficiency of detection [23,24,27,28]. Therefore, this CC-based SERS substrate remains a promising candidate for the detection of DPA. In this study, the porous CC structure is

Biomedical Optics EXPRESS

firstly decorated with large-sized AuNPs through fast vacuum annealing, subsequently followed by the assembly of small-sized AuNPs to construct a flexible SERS substrate designated as AuNPs@Au/CC. The high SERS performance of AuNPs@Au/CC substrate is assessed by the probe molecule of Rhodamine 6 G (R6 G). During the detection of the bacterial spore biomarker of DPA, the SERS substrate of AuNPs@Au/CC exhibits a linear detection range from 10^{-7} M to 10^{-13} M with a LOD of 1.58×10^{-13} M. The porous CC substrate decorated with different sizes of AuNPs can facilitate the contact of DPA molecules and enhance the Raman signal. It provides potential application for the rapid and sensitive DPA detection for preventing the biological threats. This flexible SERS substrate boasts the application in a diverse range of environments.

2. Experiment details

2.1. Chemicals and materials

Chloroauric acid ($HAuCl_4 \cdot 3H_2O$, 99.9%), Trisodium citrate dihydrate, Hydroxylamine hydrochloride, Polyvinylpyrrolidone, Cyclohexane, Ethyl alcohol, R6 G, 2, 6-pyridine dicarboxylic acid (DPA) were purchased from Xilong Chemical Co., Ltd. (Guangdong China). All the chemicals were analytical grade and used without further treatment.

2.2. Fabrication and assemble of AuNPs

AuNPs were fabricated by the seed growth method [29]. The $HAuCl_4$ solution (100 mL, 0.01% w/v) was added into a three-neck flask and placed in a heated magnetic agitator connected to a condensing tube. After heating to 100 °C, the sodium citrate dihydrate solution (2 mL, 10^{-2} g/mL) was added and stirred magnetically for 15 min until the solution changed from light yellow to garnet red. The solution cooled naturally to room temperature under reflux condensation. The prepared sol (25 mL) was added to a new three-neck flask, to which 1.0 mL of trisodium citrate dihydrate solution (10^{-2} g/mL), 1.0 mL of PVP solution (1% w/v), and 20 mL of hydroxylamine hydrochloride solution (25 mM) were added and stirred at 300 rpm. At the same time, the $HAuCl_4$ solution (20 mL, 0.1% w/v) was dripped into a new three-neck flash through a funnel and then magnetically stirred for 20 min. The solution of AuNPs was prepared upon observing a color change from garnet red to deep red and was subsequently stored in a refrigerator at 4 °C for future use.

The prepared AuNPs solution was taken and centrifuged at 6000 rpm for 10 minutes. Subsequently, the supernatant was discarded, and the nano-gold dispersion was obtained by mixing the residue with 3.0 mL of ultra-pure water. Afterward, 1.0 mL of cyclohexane was slowly introduced, allowing for a complete reaction. And then, 1.0 mL of ethanol was rapidly added. As the cyclohexane evaporated, a AuNPs thin film was finally formed on the liquid surface.

2.3. Fabrication of AuNPs@Au/CC substrate

As shown in Fig. 1(a), a thin film of AuNPs was firstly assembled on the surface of carbon cloth to form an AuNPs/CC structure, with the size of the AuNPs being about 33 nanometers. Subsequently, the prepared AuNPs/CC substrate is placed into a high-temperature vacuum annealing furnace for heating and annealing treatment. During this process, nitrogen gas is introduced as a protective gas to prevent the material from oxidizing at high temperatures. The annealing temperature is set at 900 °C, and the annealing time is 20 minutes. During this period, the AuNPs undergo recrystallization, where small-sized AuNPs particles dissolve and recrystallize into large-sized AuNPs, thus forming an Au/CC structure. As shown by the statistical analysis of 100 recrystallized AuNPs in the inset of Fig. 1(c), the diameter of the large-sized AuNPs in a range of 400-600 nm. Finally, a film of small-sized AuNPs is reassembled on the surface of the Au/CC structure to form an AuNPs@Au/CC structure, which is used as the SERS detection substrate.

Biomedical Optics EXPRESS

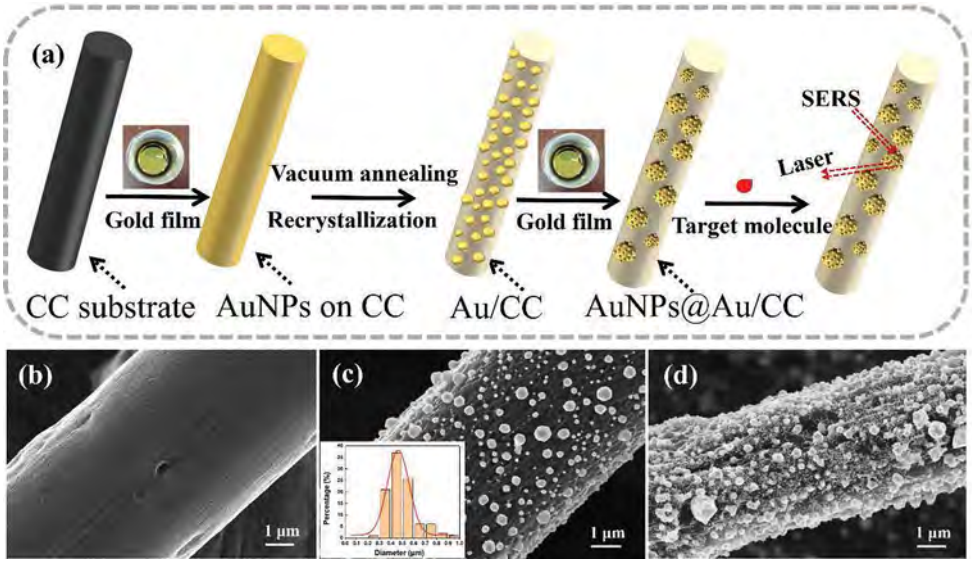

Fig. 1. (a) The flowchart shows the detailed fabrication process of the flexible SERS substrate of AuNPs@Au/CC. (b)-(d) respectively display the structural morphologies of the clean CC, Au/CC and AuNPs@Au/CC observed by SEM.

During the preparation of the SERS substrate, 900 °C is the temperature at which AuNPs melt and recrystallize under vacuum conditions. If the temperature is not high enough, the small-sized AuNPs will not melt completely, which affects the subsequent crystallization. If the temperature is too high or the annealing time is too long, gold atoms will evaporate from the surface of the carbon cloth, and large-sized AuNPs will not form.

2.4. Preparation of DPA standard solutions

The DPA powder (0.00167 g) was dissolved in 1.0 mL of ultra-pure water to prepare the aqueous solution with a concentration of 10^{-2} M. The DPA solutions with lower concentrations (10^{-3} M, 10^{-4} M, 10^{-5} M, 10^{-6} M, 10^{-7} M, 10^{-8} M, 10^{-9} M,10^{-10} M, 10^{-11} M, 10^{-12} M, 10^{-13} M and 10^{-14} M) were prepared by double dilution in turn.

2.5. Material characterization and SERS measurements

The morphology of AuNPs@Au/CC structure was characterized by scanning electron microscopy (SEM, ZEISS Sigma 300). Raman scattering was performed on the confocal Raman instrument (inVia Qontor). During SERS measurement, a laser with a wavelength of 633 nm was used as the excitation source together with a 50× objective lens at room temperature. The detection range was 100-2,000 cm^{-1}, and the acquisition time was 10 s for each Raman spectrum. Prior to detection, the baseline was calibrated to exclude fluorescent. The substrates of AuNPs@Au/CC were soaked in the analyte solutions with various concentrations. After soaking for a period of time, the substrates were removed and dried for SERS measurement.

3. Results and discussion

The SERS substrate is fabricated using assembly techniques and high-temperature vacuum annealing. Figure 1(a) illustrates the detailed fabrication process of the flexible AuNPs@Au/CC SERS substrate. Figure 1 b-d show the structural morphologies of the clean CC, Au/CC, and AuNPs@Au/CC, respectively, as observed by SEM. Figure 1(b) displays the typical carbon fiber

Biomedical Optics EXPRESS

features on the clean CC substrate. Figure 1(c) shows that small-sized AuNPs assembled on CC recrystallize into large-sized AuNPs during high-temperature vacuum annealing, forming the Au/CC structure. This structure is tightly bonded to the carbon cloth and resists detachment. The inset in Fig. 1(c) reveals that the diameters of 100 large-sized AuNPs range from approximately 400-600 nm. Figure 1(d) shows the final AuNPs@Au/CC structure, with an additional AuNPs thin film assembled onto the Au/CC surface. SEM characterization indicates that large-sized AuNPs are sparsely distributed, while small-sized AuNPs are uniformly distributed on the large-sized AuNPs and the carbon cloth surface. During the second assembly, small-sized AuNPs aggregate on the large-sized AuNPs, forming a three-dimensional core-satellite structure. The small-sized AuNPs assembled for the second time also adhere well to the Au/CC surface. Therefore, the SERS substrate based on the AuNPs@Au/CC structure is relatively stable and does not easily detach during testing. Similar to the reported core-satellite structures, this arrangement creates high-density hot spots across the surface, enhancing the local electromagnetic field strength and improving SERS signal sensitivity [30–32].

SERS technology leverages the foundational principles of traditional Raman scattering to substantially amplify the Raman signal. This amplification is attributed to the intensified electromagnetic field generated between a metallic surface (Au, Ag, Cu) and the sample being analyzed [33]. This enhancement empowers SERS to boast a diverse range of applications, capable of precisely identifying even trace amounts of biological and hazardous chemicals [22]. Furthermore, its significance extends to medical diagnosis [34–36] and food safety detection [37,38], underscoring its vital importance in these fields. Figure 2(a) presents the large-scale SEM image of AuNPs@Au/CC, enabling a clear visualization of the entire substrate's morphology. Figure 2(b)–2(d) show the detailed structure in different regions. The surface of the recrystallized large-sized AuNPs can be adorned with assembled small-sized AuNPs, irrespective of whether they are positioned at the center (Fig. 2(b)) or near the edge (Fig. 2(c)) of the carbon fiber. As shown in Fig. 2(d), the assembled small-sized AuNPs are also uniformly dispersed on the areas devoid of large-sized AuNPs. It is suggested that the AuNPs not only adhere to the large-sized AuNPs but also establish a consistent coating layer across the carbon cloth surface. So that, the SERS substrate exhibits high sensitivity and specificity in the detection of targets molecules.

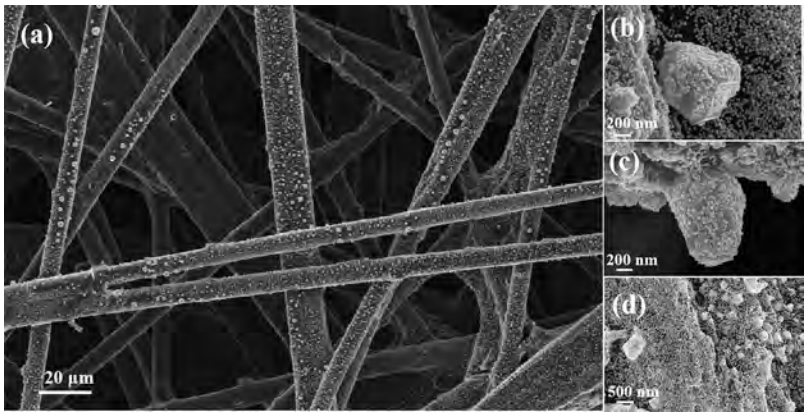

Fig. 2. Characteristics of AuNPs@Au/CC : (a) presents the large-scale SEM image of AuNPs@Au/CC. (b)-(d) show the detailed structure in different regions.

R6 G has been selected as the probe molecule for evaluating the sensitivity of the fabricated AuNPs@Au/CC SERS substrate, with the concentration ranging from 10^{-6} M to 10^{-13} M. During the detection process, there is a substantial variation in the SERS signal intensity of R6 G across different regions. Figure 3(a) displays SERS spectra from regions with large AuNPs

Biomedical Optics EXPRESS

(AuNPs@Au/CC), while Fig. 3(b) shows spectra from regions without large AuNPs (AuNPs/CC). In Fig. 3(a) and 3(b), it is difficult to discern the order-of-magnitude difference in Raman signal intensity between the two difference detection regions. To quantitatively assess the enhancement effect, Fig. 3(c) compares Raman peak intensities at 615 cm^{-1} and 775 cm^{-1} for 10^{-11} M R6 G in both regions. In the large-sized AuNPs region (region 1), the intensities are 4361 and 2998, respectively. In the region without large-sized AuNPs (region 2), the intensities are 743 and 290, respectively. This difference confirms the contribution of large-sized AuNPs to SERS signal amplification. This is because its core-satellite structure enhances the local electromagnetic field strength, thereby improving the sensitivity of the SERS signal [30–32]. During testing, the large-sized AuNPs region is easily identifiable under an optical microscope and shows much better SERS performance than the small-sized AuNPs directly loaded on the carbon cloth surface.

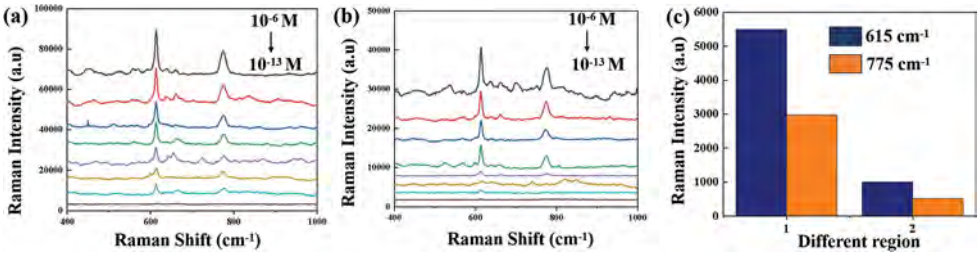

Fig. 3. SERS properties of R6 G in different regions based on AuNPs@Au/CC: (a) displays the SERS signal intensity of R6 G, as measured on the surface of AuNPs@Au/CC. (b) depicts the SERS signal intensity of R6 G in an area devoid of large gold particles. (c) depicts the compared results of the SERS signal intensity of of R6 G between the two regions (region 1 represents the large-sized AuNPs area; region 2 represents the area without large-sized AuNPs) at the concentration of 10^{-11} M.

After being evaluated with the R6 G molecule, the AuNPs@Au/CC substrate can be utilized for the SERS detection of DPA. Figure 4(a) displays the Raman characteristics of DPA molecule, exhibiting the prominent peaks at 652 cm^{-1}, 764 cm^{-1}, 1003 cm^{-1}, 1161 cm^{-1}, 1290 cm^{-1}, 1457 cm^{-1}, 1583 cm^{-1}, and 1649 cm^{-1}. The spectral peaks obtained in this study are consistent with the data reported in the literature [39]. Among these peaks, the Raman peaks of DPA located at 652 cm^{-1}, 1003 cm^{-1}, and 1161 cm^{-1} correspond respectively to the CC ring bending mode, the CC stretching symmetric ring breathing modes, and the CH-bending modes [22]. In particular, the peak located at 1003 cm^{-1} serves as a typical Raman characteristic peak for the detection of DPA. Figure 4(b) shows the Raman spectra of DPA (10^{-8} M) observed by AuNPs@Au/CC, AuNPs/CC and AuNPs/Si substrates, respectively. Figure 4(c) compares the Raman peak intensities at 1003 cm^{-1} for the three substrates shown in Fig. 4(b). A distinct DPA peak appears at 1003 cm^{-1} on the AuNPs@Au/CC substrate, with intensity exceeding that of AuNPs/CC. In contrast, no detectable peak is observed on the AuNPs/Si substrate. These results confirm the enhanced SERS detection capability of the flexible AuNPs@Au/CC substrate for DPA.

Moreover, the SERS effect of AuNPs@Au/CC substrate can be analyzed by the analytical enhancement factor (AEF), which is calculated by the formula of $I_{SERS} \times C_{RS}/I_{RS} \times C_{SERS}$ based on the Raman peak intensity at 1003 cm^{-1} [40]. In the formula, I_{SERS} represents the Raman peak intensity of DPA on AuNPs@Au/CC substrate, C_{SERS} is the concentration of DPA (10^{-8} M) on AuNPs@Au/CC substrate, I_{RS} represents the Raman peak intensity of DPA on the bare carbon cloth, C_{RS} is the concentration of DPA (10^{-3} M) on the bare carbon cloth. According to the calculation, the AEF value of AuNPs@Au/CC SERS substrate is 4.4×10^6, which further confirms the good Raman enhancement capability

Biomedical Optics EXPRESS

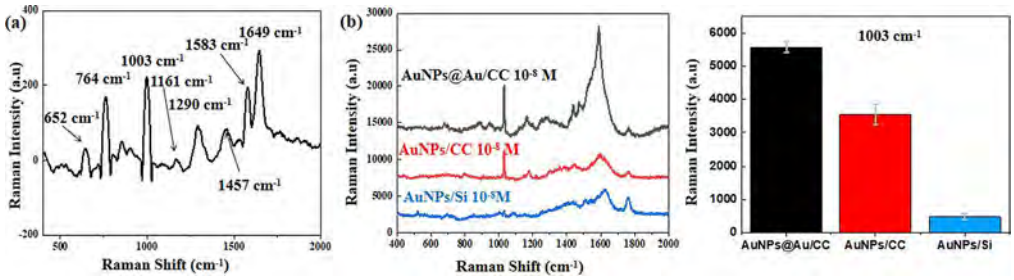

Fig. 4. (a) displays the Raman characteristics of DPA molecule, exhibiting the prominent peaks at 652 cm^{-1}, 764 cm^{-1}, 1003 cm^{-1}, 1161 cm^{-1}, 1290 cm^{-1}, 1457 cm^{-1}, 1583 cm^{-1}, and 1649 cm^{-1}. (b) presents the Raman spectra of DPA (10^{-8} M) acquired from both AuNPs@Au/CC, AuNPs/CC and AuNPs/Si substrates, respectively. (c) shows the Raman peak intensities corresponding to the three different substrates depicted in (b).

Figure 5(a) depicts the SERS spectra, which are acquired from the eight different concentrations of DPA. The Raman peak intensity at 1003 cm^{-1} is prominent, which is chose for the quantitative analysis. The Raman peaks of DPA remain distinctive detectable even at the low concentration of 10^{-13} M. The trend demonstrates a decreasing trend as the DPA concentration ranges from 10^{-7} M to 10^{-14} M. Figure 5(b) displays the direct proportionality between the Raman intensity at 1003 cm^{-1} and the concentration of DPA solution, as evidenced by the spectra in Fig. 5(a). The linear equation is calculated as $y = 9311 + 705x$, $R^2 = 0.992$, indicating a good linear correlation between Raman intensity and DPA concentration. The equation 3Sd/k is employed to calculate the LOD of the AuNPs@Au/CC SERS substrate [23]. In the equation, Sd represents the standard deviation of 5 times the signal intensity measured from the blank substrate, and k represents the slope of the linear plot depicted in Fig. 5(b). Consequently, the LOD of the AuNPs@Au/CC SERS substrate is calculated as 1.58×10^{-13} M. The result confirms the high sensitivity of the AuNPs@Au/CC SERS substrate, underscoring the feasibility of its application in quantitative analysis.

The reproducibility and stability of the Raman signal are equally crucial factors in assessing the effectiveness of SERS substrate. In this experiment, 10 different regions are randomly selected for the measurement to confirm the reproducibility of the AuNPs@Au/CC SERS substrate. Figure 5(c) shows the three-dimensional diagram of the SERS spectra of DPA, which are captured at at the concentration of 10^{-8} M in these 10 regions. Figure 5(d) shows the corresponding Raman peak intensity and its relative standard deviation (RSD) value. The results show that the RSD value of the DPA Raman peak at 1003 cm^{-1} is 10.2%, proving the good reproducibility of the AuNPs@Au/CC SERS substrate.

Figure 6 shows the statistical data of DPA detection performance containing SERS and other techniques [41,42]. As compared, the AuNPs@Au/CC SERS substrate developed in this study shows the lowest LOD of 1.58×10^{-13} M and a linear detection range from 10^{-7} M to 10^{-13} M. It is demonstrated that the AuNPs@Au/CC sensor exhibits high sensitivity within its effective linear range compared to other reported sensing platforms. In this study, we fabricated the AuNPs@Au/CC core-satellite structure. This structure can enhance the signal, thereby improving the detection sensitivity [30–32]. Meanwhile, the target region can be quickly located under an optical microscope, which further improves the detection efficiency. However, the current method has certain limitations, the uneven size distribution of the large-sized AuNPs may influence the reproducibility of the substrate.

In order to evaluated the long-term stability in conventional analysis, the SERS activity of AuNPs@Au/CC after storage in air for a period of time is further tested. The Au/CC structure is formed through high-temperature annealing and recrystallization, creating a very stable structure

Biomedical Optics EXPRESS

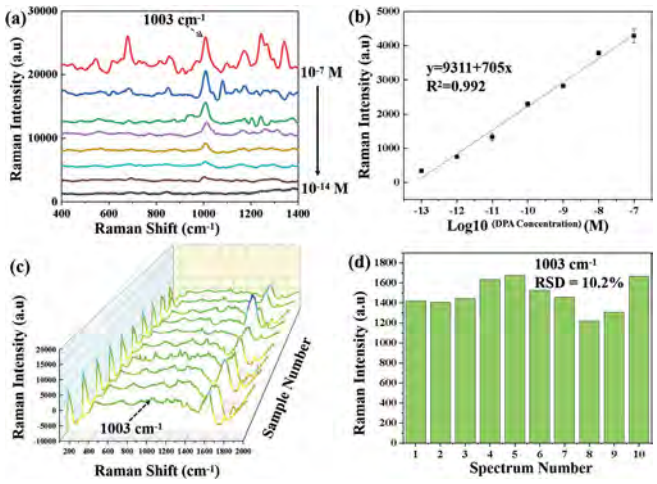

Fig. 5. DPA SERS detection for AuNPs@Au/CC: (a) depicts the SERS spectra, which are acquired from the eight different concentrations of DPA. (b) Logarithm of DPA concentration and Raman intensity at 1003 cm^{-1} (error bar represents standard deviation of three measurements). (c) shows the three-dimensional diagram of the SERS spectra of DPA, which are captured at at the concentration of 10^{-8} M in these 10 regions; (d) shows the corresponding Raman peak intensity and its relative standard deviation (RSD) value.

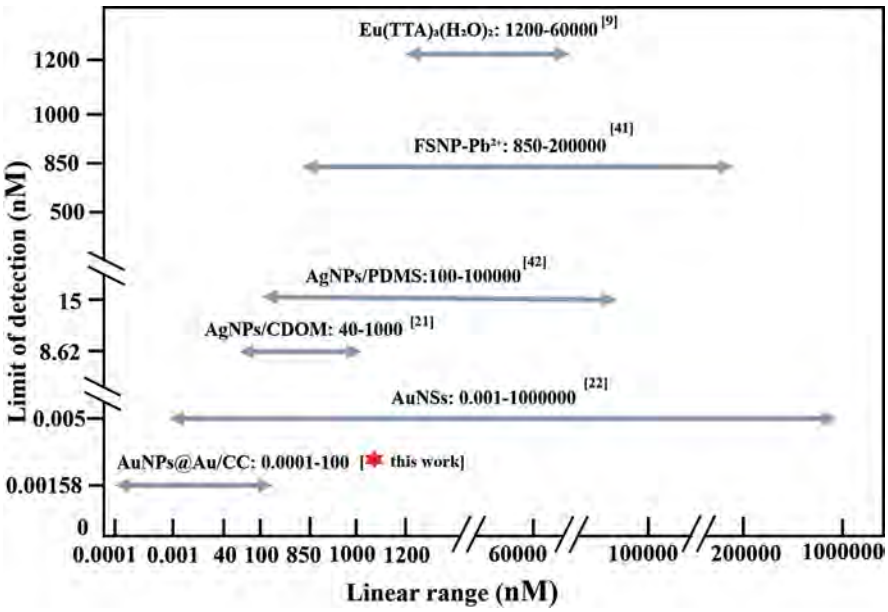

Fig. 6. shows the comparison of DPA detection performance between AuNPs@Au/CC and other surface-enhanced Raman scattering (SERS) substrates, as well as other detection techniques.

Biomedical Optics EXPRESS

as the large-sized AuNPs bond tightly with the carbon cloth substrate. The small-sized AuNPs assembled for the second time also adhere well to the Au/CC surface. Therefore, the SERS substrate based on the AuNPs@Au/CC structure is relatively stable and does not undergo significant changes due to temperature, humidity, or storage time during testing. Figure 7(a) shows the SERS spectra of DPA (10^{-8} M) on the same substrate over different storage periods, with Fig. 7(b) quantifying the corresponding Raman peak intensities at 1003 cm^{-1}. The Raman characteristic peak intensity for the storage time of 1 day and 5 days remains consistent under room temperature and atmospheric conditions, indicating good short-term stability. When the storage time is extended to 10 days, a slight decrease in the characteristic peak intensity occurs. This suggests that the SERS activity of the substrate will gradually diminish over time. During storage, oxidation of the substrate surface or adsorption of other foreign substances may occur, leading to a reduction in its activity. Thus, for SERS substrates that require long-term storage, appropriate protective measures should be considered, such as vacuum packaging or the addition of a protective layer, to extend their service life and maintain stable SERS performance [43]. As shown in Fig. 7(c), the reproducibility of four substrates prepared in different batches has been assessed. The Raman peak intensities at 1003 cm^{-1} shows little changes at the DPA concentration of 10^{-8} M, and the calculated batch-to-batch reproducibility by RSD is 15.9%. These results indicate that the SERS substrate has potential for applications in real-time detection.

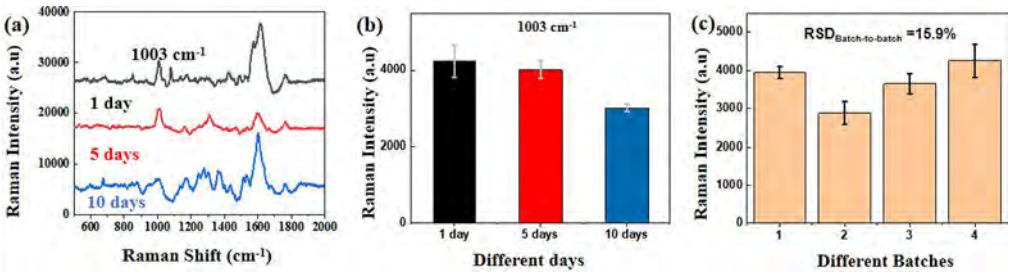

Fig. 7. AuNPs@Au/CC stability of SERS substrates: (a) shows the SERS spectra of DPA at 1003 cm^{-1} for the substrate under different storage times. (b) represents the Raman peak intensities at 1003 cm^{-1} from Fig. 7(a) under different storage times (n = 3). (c) shows the batch-to-batch reproducibility of Raman peak intensities at 1003 cm^{-1} for substrates prepared in different batches, tested at a concentration of 10^{-8} M (n = 3).

Compared with traditional fluorescence detection techniques, SERS technology has more significant advantages in DPA detection. SERS technology eliminates the need for complex fluorescence labeling steps and avoids the use of fluorescent probes and their potential background interference issues, thus offering greater advantages in terms of operational simplicity and detection cost. Since SERS signals are based on the fingerprint spectra of molecular vibrations, the Raman characteristic peaks are less susceptible to fluorescence quenching effects, ensuring the stability and reliability of the detection signals. Carbon-based SERS substrates reported in prior studies often suffer from trade-offs between sensitivity, cost, and fabrication complexity. For example, AgNPs@TiO_2/CFC substrates synthesized via UV reduction exhibit a detection limit of 10^{-9} M, but require stringent control over solution parameters and irradiation conditions [44]. Similarly, magnetron-sputtered MWNTs/AgNPs substrates achieve 10^{-10} M sensitivity, yet depend on costly vacuum systems and multi-step processes [45]. In contrast, the AuNPs@Au/CC substrate utilizes a high-temperature vacuum annealing strategy to induce AuNP recrystallization. During this process, small-sized AuNPs dissolve and reprecipitate as large-sized AuNPs, forming a robust Au/CC structure. Subsequently, a secondary layer of AuNPs film is assembled on the Au/CC surface, ultimately form an AuNPs@Au/CC structure. During the detection of DPA, the

Biomedical Optics EXPRESS

SERS substrate of AuNPs@Au/CC exhibits a LOD of 1.58×10^{-13} M at the detection range from 10^{-7} M to 10^{-13} M.

This study demonstrates that the gold film decoration method offers significant advantages over conventional AuNPs modification techniques in terms of simplicity and scalability. While traditional approaches like solution immersion require meticulous optimization of nanoparticle concentration and immersion duration [31], and plasma sputtering depends on specialized high-vacuum equipment [46]. Liquid-gas interfacial self-assembly strategy enables rapid and uniform AuNPs deposition through a more streamlined process. The protocol concentrates AuNPs at the cyclohexane/ethanol interface followed by direct transfer to carbon cloth substrates, eliminating the need for complex instrumentation and additional chemical treatments. This synergistic approach capitalizes on the inherent benefits of flexible, low-cost carbon cloth while leveraging the enhanced efficiency of interfacial self-assembly, ultimately establishing the gold film decoration technique as a highly promising solution for practical SERS applications.

4. Conclusion

In conclusion, the flexible SERS substrate of AuNPs@Au/CC is fabricated to realize the high sensitive detection of the bacterial spore biomarker of DPA. The porous CC surface is firstly decorated with large-sized AuNPs through fast vacuum annealing, subsequently followed by the assembly of small-sized AuNPs to construct a flexible SERS substrate of AuNPs@Au/CC. The porous CC substrate decorated with different sizes of AuNPs can facilitate the contact of molecules and enhance the Raman signal. The high SERS performance of AuNPs@Au/CC is assessed by the probe molecule of R6 G. During the detection of DPA, the SERS substrate of AuNPs@Au/CC exhibits a linear detection range from 10^{-7} M to 10^{-13} M with a LOD of 1.58×10^{-13} M. The high performance of the flexible SERS substrate provides a new possibility for the rapid and sensitive DPA detection. It holds significance in preventing the biological threats, boasting the potential application in a diverse range of environments.

Funding. Natural Science Foundation of Hainan Province (521RC555).

Acknowledgments. The SERS measurements were provided by the Key Laboratory of Hainan Trauma and Disaster Rescue at Hainan Medical University, and the authors were grateful to Rui Wang.

Disclosures. The authors declare that there are no conflicts of interest related to this article.

Data availability. Data underlying the results presented in this paper are not publicly available at this time but may be obtained from the authors upon reasonable request.

Reference

1. T. T. Gong, S. Yang, M. Li, *et al.*, "Dual-ligand-functionalized dodeca-nuclear lanthanide-tungsten-cluster incorporated selenotungstates and fluorescence detection of dipicolinic acid (an anthrax biomarker)," Inorg. Chem. Front. **10**(9), 2799–2810 (2023).
2. M. Na, S. Liu, J. Ma, *et al.*, "Determination of pathogenic bacteria-Bacillus anthrax spores in environmental samples by ratiometric fluorescence and test paper based on dual-emission fluorescent silicon nanoparticles," J. Hazard. Mater. **386**, 121956 (2020).
3. Y. Y. Ma, Z. J. Wang, and D. J. Qian, "Ratiometric fluorescence detection of anthrax biomarker based on terbium (III) functionalized graphitic carbon nitride nanosheets," Talanta **230**, 122311 (2021).
4. Q. Zhou, Y. Fang, J. Li, *et al.*, "A design strategy of dual-ratiomentric optical probe based on europium-doped carbon dots for colorimetric and fluorescent visual detection of anthrax biomarker," Talanta **222**, 121548 (2021).
5. M. Enserink, "Biodefense hampered by inadequate tests," Science **294**(5545), 1266–1267 (2001).
6. P. Zhang, A. Ni, J. Zhang, *et al.*, "Tb-MOF-based luminescent recovery probe for rapid and facile detection of an anthrax biomarker," Sens. Actuators, B **384**, 133624 (2023).
7. A. K. Goel, "Anthrax: A disease of biowarfare and public health importance," World. J. Clin. Cases **3**(1), 20 (2015).
8. T. N. Huan, T. Ganesh, S. H. Han, *et al.*, "Sensitive detection of an Anthrax biomarker using a glassy carbon electrode with a consecutively immobilized layer of polyaniline/carbon nanotube/peptide," Biosens. Bioelectron **26**(10), 4227–4230 (2011).
9. Z. Abbas and A. K. Patra, "Luminescent β-diketonate coordinated europium(III) sensor for rapid and sensitive detection of Bacillus Anthracis biomarker," J. Lumin. **244**, 118726 (2022).

Biomedical Optics EXPRESS

10. M. D. Yilmaz and H. A. Oktem, "Eriochrome black T-Eu3 + complex as a ratiometric colorimetric and fluorescent probe for the detection of dipicolinic acid, a biomarker of bacterial spores," Anal. Chem. **90**(6), 4221–4225 (2018).
11. N. Morel, H. Volland, J. Dano, *et al.*, "Fast and sensitive detection of bacillus anthracis spores by immunoassay," Appl. Environ. Microbiol. **78**(18), 6491–6498 (2012).
12. J. Kim and M. Y. Yoon, "Recent advances in rapid and ultrasensitive biosensors for infectious agents: lesson from bacillus anthracis diagnostic sensors," Analyst **135**(6), 1182 (2010).
13. D. Li, A. D. Rands, S. C. Losee, *et al.*, "Automated thermochemolysis reactor for detection of bacillus anthracis endospores by gas chromatography–mass spectrometry," Anal. Chim. Acta. **775**, 67–74 (2013).
14. D. Li, T. V. Truong, T. M. Bills, *et al.*, "GC/MS method for positive detection of bacillus anthracis endospores," Anal. Chem. **84**(3), 1637–1644 (2012).
15. S. Nizkorodova, E. R. Mal'tseva, Z. A. Berdygulova, *et al.*, "Real-time PCR detection of bacillus anthracis by lambda-ba03 prophage genes," Probl. P. D. Infect. **3**(3), 170–172 (2022).
16. P. Braun, M. D. Nguyen, M. C. Walter, *et al.*, "Ultrasensitive detection of bacillus anthracis by real-time PCR targeting a polymorphism in multi-copy 16S rRNA genes and their transcripts," Int. J. Mol. Sci. **22**(22), 12224 (2021).
17. Z. Cheng, X. Liu, S. Q. Zhang, *et al.*, "Placeholder strategy with upconversion nanoparticles-eriochrome black T conjugate for a colorimetric assay of an anthrax biomarker," Anal. Chem. **91**(18), 12094–12099 (2019).
18. Z. Cong, M. Zhu, Y. Zhang, *et al.*, "Three novel metal-organic frameworks with different coordination modes for trace detection of anthrax biomarkers," Dalton Trans. **51**(1), 250–256 (2021).
19. S. Yin and C. Tong, "Europium(III)-modified silver nanoparticles as ratiometric colorimetric and fluorescent dual-mode probes for selective detection of dipicolinic acid in bacterial spores and lake waters," ACS Appl. Nano Mater. **4**(5), 5469–5477 (2021).
20. K. Luan, R. Meng, C. Shan, *et al.*, "Terbium functionalized micelle nanoprobe for ratiometric fluorescence detection of anthrax spore biomarker," Anal. Chem. **90**(5), 3600–3607 (2018).
21. G. Jiang, W. Xu, X. Huang, *et al.*, "Detection of bacillus cereus spore biomarkers using SERS-based cuttlebone-derived organic matrix/silver nanoparticles," ACS Sustainable Chem. Eng. **11**(10), 4145–4154 (2023).
22. T. K. Naqvi, A. Bajpai, M. S. S. Bharati, *et al.*, "Ultra-sensitive reusable SERS sensor for multiple hazardous materials detection on single platform," J. Hazard. Mater. **407**, 124353 (2021).
23. N. R. Barveen, S. Chinnapaiyan, T. Wang, *et al.*, "Photochemical decoration of gold nanoparticles on MoS2 nanoflowers grafted onto the flexible carbon cloth as a recyclable SERS sensor for the detection of antibiotic residues on curved surfaces," Chemosphere **346**, 140677 (2024).
24. S. Yao, Y. Lv, Q. Wang, *et al.*, "Facile preparation of highly sensitive SERS substrates based on gold nanoparticles modified graphdiyne/carbon cloth," Appl. Surf. Sci. **609**, 155098 (2023).
25. J. Zhu, J. Luo, Z. Hua, *et al.*, "SERS microfluidic chip integrated with double amplified signal off-on strategy for detection of microRNA in NSCLC," Biomed. Opt. Express **15**(2), 594 (2024).
26. S. Zhang, F. Chen, Y. Zhang, *et al.*, "SERS detection platform based on a nucleic acid aptamer-functionalized Au nano-dodecahedron array for efficient simultaneous testing of colorectal cancer-associated microRNAs," Biomed. Opt. Express **15**(5), 3366 (2024).
27. S. Meng, J. Liang, W. Jia, *et al.*, "Metal-free and flexible surface-enhanced Raman scattering substrate based on oxidized carbon cloth," Carbon **189**, 152–161 (2022).
28. S. Lu, T. You, N. Yang, *et al.*, "Flexible SERS substrate based on Ag nanodendrite–coated carbon fiber cloth: simultaneous detection for multiple pesticides in liquid droplet," Anal. Bioanal.Chem. **412**(5), 1159–1167 (2020).
29. D. Tu, A. Holderby, and G. Coté, "Aptamer-based surface-enhanced resonance raman scattering assay on a paper fluidic platform for detection of cardiac troponin," J. Biomed. Opt. **25**(09), 097001 (2020).
30. S. H. Mao, F. B. Pei, S. S. Feng, *et al.*, "Detection of trace Rhodamine B using stable, uniformity, and reusable SERS substrate based on Ag@SiO_2-Au nanoparticles," Colloids Surf., A **657**, 130595 (2023).
31. Y. Li, X. L. Xin, T. T. Zhang, *et al.*, "Raspberry-like polyamide@Ag hybrid nanoarrays with flexible cores and SERS signal enhancement strategy for adenosine detection," Chemical Engineering Journal **422**, 129983 (2021).
32. H. Liu, Y. Li, J. Dykes, *et al.*, "Manipulating the functionalization surface of graphene-encapsulated gold nanoparticles with single-walled carbon nanotubes for SERS sensing," Carbon **140**, 306–313 (2018).
33. S. Kumar, K. Tokunaga, K. Namura, *et al.*, "Experimental evidence of two-fold electromagnetic enhancement mechanism of surface-enhanced raman scattering," J. Phys. Chem. C **124**(38), 21215–21222 (2020).
34. M. Benešová, S. Bernatová, F. Mika, *et al.*, "SERS-tags: selective immobilization and detection of bacteria by strain-specific antibodies and surface-enhanced raman scattering," Biosensors **13**(2), 182 (2023).
35. C. Qiu, W. Zhang, Y. Zhou, *et al.*, "Highly sensitive surface-enhanced Raman scattering (SERS) imaging for phenotypic diagnosis and therapeutic evaluation of breast cancer," Chem. Eng. J. **459**, 141502 (2023).
36. J. J. S. Rickard, V. Di-Pietro, D. J. Smith, *et al.*, "Rapid optofluidic detection of biomarkers for traumatic brain injury via surface-enhanced raman spectroscopy," Nat. Biomed. Eng. **4**(6), 610–623 (2020).
37. H. Li, E. Dumont, R. Slipets, *et al.*, "Democratizing robust SERS nano-sensors for food safety diagnostics," Chem. Eng. J. **470**, 144023 (2023).
38. B. Li, S. Liu, L. Huang, *et al.*, "Nanohybrid SERS substrates intended for food supply chain safety," Coord. Chem. Rev. **494**, 215349 (2023).
39. H. W. Cheng, S. Y. Huan, H. L. Wu, *et al.*, "Surface-enhanced raman spectroscopic detection of a bacteria biomarker using gold nanoparticle immobilized substrates," Anal. Chem. **81**(24), 9902–9912 (2009).

Biomedical Optics EXPRESS

40. M. K. Francis, B. K. Sahu, P. B. Bhargav, *et al.*, "Ag Nanowires Based SERS Substrates with Very High Enhancement Factor," Phys. E **137**, 115080 (2022).
41. Y. N. Cetinkaya, O. Bulut, H. A. Oktem, *et al.*, "Fluorescent silica nanoparticles as nano-chemosensors for the sequential detection of Pb^{2+} ions and bacterial-spore biomarker dipicolinic acid (DPA) in aqueous solution," Spectrochim. Acta, Part A **303**, 123222 (2023).
42. M. Y. Ge, W. F. Zhao, Y. Han, *et al.*, "Contactless and robust dielectric microspheres-assisted surface-enhanced Raman scattering sensitivity improvement for anthrax biomarker detection," Front. Chem. **10**, 1–9 (2022).
43. S. Limwichean, H. Nakajima, T. Lertvanithphol, *et al.*, "Self-depositing passivation layer investigations on stability improvement of the Ag NRs SERS substrate," Vacuum **196**, 110734 (2022).
44. N. Sun, B. Huang, Z. Y. Lv, *et al.*, "UV-catalyzed TiO2–based optofluidic SERS chip for three online strategies: fabrication, detection, and self-cleaning," Anal. Chem. **96**(22), 9104–9112 (2024).
45. J. Zhang, X. L. Zhang, S. M. Chen, *et al.*, "Surface-enhanced Raman scattering properties of multi-walled carbon nanotubes arrays-Ag nanoparticles," Carbon **100**, 395–407 (2016).
46. M. L. Wang, Y. H. Wang, X. Y. Yan, *et al.*, "Three-dimensional hierarchical reticular nanostructure of fulfora candelaria wing decorated by Ag nanoislands as practical SERS-active substrates," Nanomaterials **8**(11), 905 (2018).